JBC ARTICLE

⌘ Author's Choice

Two clusters of surface-exposed amino acid residues enable high-affinity binding of retinal degeneration-3 (RD3) protein to retinal guanylyl cyclase

Received for publication, April 7, 2020, and in revised form, June 2, 2020 Published, Papers in Press, June 3, 2020, DOI 10.1074/jbc.RA120.013789

Igor V. Peshenko and Alexander M. Dizhoor*

From the Pennsylvania College of Optometry, Salus University, Elkins Park, Pennsylvania, USA

Edited by Henrik G. Dohlman

Retinal degeneration-3 (RD3) protein protects photoreceptors from degeneration by preventing retinal guanylyl cyclase (RetGC) activation via calcium-sensing guanylyl cyclase–activating proteins (GCAP), and RD3 truncation causes severe congenital blindness in humans and other animals. The three-dimensional structure of RD3 has recently been established, but the molecular mechanisms of its inhibitory binding to RetGC remain unclear. Here, we report the results of probing 133 surface-exposed residues in RD3 by single substitutions and deletions to identify side chains that are critical for the inhibitory binding of RD3 to RetGC. We tested the effects of these substitutions and deletions *in vitro* by reconstituting purified RD3 variants with GCAP1-activated human RetGC1. Although the vast majority of the surface-exposed residues tolerated substitutions without loss of RD3's inhibitory activity, substitutions in two distinct narrow clusters located on the opposite sides of the molecule effectively suppressed RD3 binding to the cyclase. The first surface-exposed cluster included residues adjacent to Leu^{63} in the loop connecting helices 1 and 2. The second cluster surrounded Arg^{101} on a surface of helix 3. Single substitutions in those two clusters drastically, *i.e.* up to 245-fold, reduced the IC_{50} for the cyclase inhibition. Inactivation of the two binding sites completely disabled binding of RD3 to RetGC1 in living HEK293 cells. In contrast, deletion of 49 C-terminal residues did not affect the apparent affinity of RD3 for RetGC. Our findings identify the functional interface on RD3 required for its inhibitory binding to RetGC, a process essential for protecting photoreceptors from degeneration.

The RD3 (retinal degeneration-3), a 23-kDa 195-residue protein (1, 2), plays two essential roles in photoreceptors. Firstly, RD3 enhances accumulation of retinal membrane guanylyl cyclase (RetGC) in rod and cone outer segments (3–6) and thus enables regulation of cGMP production in the outer segment required for phototransduction. The two RetGC isozymes RetGC1 *(GUCY2D)* and, to a lesser extent, RetGC2 (*GUCY2F*) (7–10), allow vertebrate photoreceptors to maintain inward ion current via cGMP-gated channels in the outer segments. After illumination, when light-stimulated phosphodiesterase activity forces cGMP-gated channels to close, RetGC in the outer segment becomes accelerated by Ca^{2+}/Mg^{2+} sensor proteins (GCAPs) (11–17) to replenish cGMP and thus expedite photoreceptor recovery from excitation and adaption to light (reviewed in Refs. 18–21). Secondly, RD3, which is predominantly located in the inner segments of photoreceptors (5, 6, 22), strongly inhibits the cyclase by suppressing its basal and GCAP-stimulated activity (23, 24). The inhibitory binding of RD3 competing with GCAPs for the cyclase is required for preventing photoreceptor degeneration (6), and the lack of such binding causes the congenital retinal blindness because of rapid loss of rods and cones (6, 22, 24). Deletions of RD3 have been linked to a severe recessive degenerative blindness, Leber's congenital amaurosis 12 (LCA12) in human patients (1, 25) (Fig. 1) and *rd3* retinal degeneration in mice (1). A frameshift in RD3 has also been linked to inherited canine retinal dysplasia (26). Recent studies argue that the rapid death of photoreceptors lacking RD3 primarily results not from reduction of RetGC content in the outer segment (24), but from the lack of the RD3 inhibitory activity counteracting GCAP-dependent activation of the remaining cyclase, likely in the inner segment (6, 24). The molecular mechanisms of RD3/RetGC interaction, despite its importance for photoreceptor function and survival, remain unclear because of insufficient structural and functional data. The molecular structure of RetGC remains largely unknown and mutational analysis of the cyclase presents a major challenge because of the larger size of the enzyme and the complexity of its regulation. Another major challenge presents high propensity of RD3 to precipitate at concentrations required for structural analyses (24, 27). However, the three-dimensional structure of RD3 core, an elongated bundle of four α-helices (Fig. 1), was recently established using a soluble variant of RD3 that retained attenuated affinity for the cyclase (27). The preliminary testing of several fragments in RD3 primary structure that contained surface-exposed and buried in the core structure residues indicated that the cyclase-binding interface on RD3 includes the central portion of the helical bundle (Fig. 1) and that the part of the bundle forming the functional interface with the cyclase involves helices 3 and 4 (24, 27). Nonetheless, the identities of the residues on the surface of RD3 that are essential for its functional contact with the cyclase remained unclear, in part because the full-size RD3 remains unsuitable for structural analyses. In the present study, we functionally probed by mutations 133 residues circumventing the entire surface of the RD3 molecule, both of the central core and the predicted unstructured parts of the protein. We identified two narrow surface-exposed clusters responsible for the inhibitory binding of RD3

* For correspondence: Alexander M. Dizhoor, adizhoor@salus.edu.

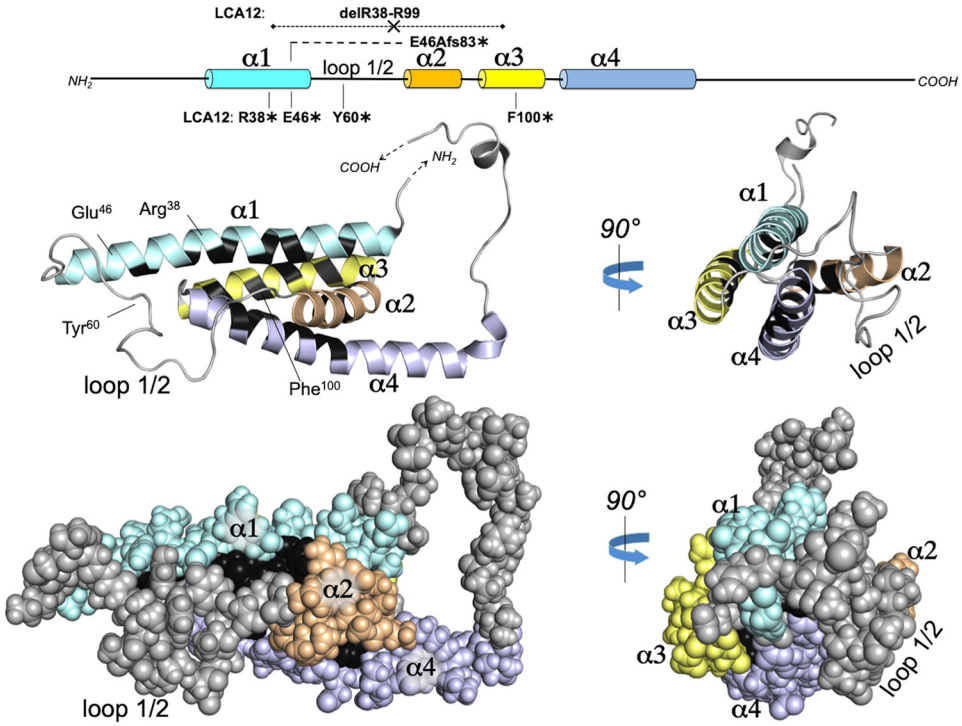

Figure 1. Residues in RD3 targeted for mutational analysis. The *top* diagram presents the schematics of RD3 polypeptide structure comprised of four α-helices *(cylinders* α1 through α 4) connected to unstructured regions (*straight line*). Recessive mutations in RD3 linked to LCA12 include nonsense mutants *R38**, *E46**, *Y60**, *F100**, a two-base deletion causing a frameshift at the residue 46 and premature termination downstream (*E46Afs83**), and an aberrant splicing resulting in deletion of the residues 38–99 (1, 25, 42). Positions of the residues replaced by the LCA12 nonsense mutations are also indicated in the three-dimensional structure of the RD3 α-helical bundle (27) presented as a *ribbon diagram* (*middle*). Filled-spheres diagram of the structure (*bottom*) depicts the location of the surface-exposed (colors matching that of the corresponding helices in the primary structure diagram) *versus* that of the buried residues (*black*) in the three-dimensional structure. The surface-exposed residues were subjected to the mutational analysis as further described in this study.

to the cyclase. One of the clusters was located on the surface of α-helix 3. The other cluster critical for the inhibitory binding was found on the opposite side of the molecule, in the loop connecting α-helices 1 and 2. This study presents the first high-resolution functional map of RD3 as a guanylyl cyclase regulating protein.

Results

Mutations in two clusters of surface-exposed residues suppress RD3 ability to inhibit RetGC1

To functionally locate the surface-exposed residues critically important for the inhibitory binding of RD3 to guanylyl cyclase, we first scanned the entire surface of the molecule (Fig. 1) with single-residue substitutions that altered the properties of the residues but did not fully revert their main properties, *e.g.* the hydrophilic residues were substituted with other hydrophilic residues of the opposite charge (such as Lys or Arg to Glu and vice versa) or of different sizes of the side chain, but not with strongly hydrophobic residues, to minimize the potential of affecting the overall fold of the protein. Conversely, hydrophobic side chains were changed to hydrophobic residues of different sizes. In some cases, they were replaced by more hydrophilic residues, but only if the original hydrophobic side chains were already exposed on the surface in the RD3 core three-dimensional structure (Fig. 1). We avoided making substitutions in side chains directed inside the structure (shown in *black* in Fig. 1) to minimize possible effects on the overall fold and/or changing distances between helices in the α-helical bundle of the core by creating steric hindrances.

All expressed RD3 mutants purified from *Escherichia coli* were tested in a standard primary screening assay by being reconstituted with HEK293 membranes containing recombinant human guanylyl cyclase RetGC1 (6, 23, 24). The reason we chose to use a recombinant RetGC instead of retinal preparations in this study was 2-fold. First, the native RetGC activity in photoreceptor membranes lacking the endogenous RD3 (which could otherwise skew the effects of the added recombinant RD3), such as isolated from rd3/rd3 mice (1), is so drastically decreased (6, 24) that the accurate measurements of its additional inhibition by the exogenous recombinant RD3 becomes less reliable because of larger margins of error. Second, RetGC from normal photoreceptors already containing the endogenous RD3 cannot be separated from the RD3 by being extracted in the presence of detergent without a complete loss of the cyclase regulation after the extraction (28). In contrast, the recombinant RetGC1 expressed in HEK293 cells lacking the endogenous RD3 retains its regulation by GCAP and RD3, as demonstrated earlier in multiple studies (6, 7, 23, 24, 27, 29).

The recombinant human RetGC1 in the standard assay was pre-activated by 1.5 μM Mg^{2+} GCAP1 in the presence of 2 mM EGTA and saturating 10 mM Mg^{2+} (30, 31). For the initial comparison of the inhibitory activity to that of the WT, the suppression of RetGC1/GCAP complex by WT RD3 and its mutants was assayed at a standard 100 nM RD3, the concentration at which the WT RD3 suppressed the activity of the cyclase

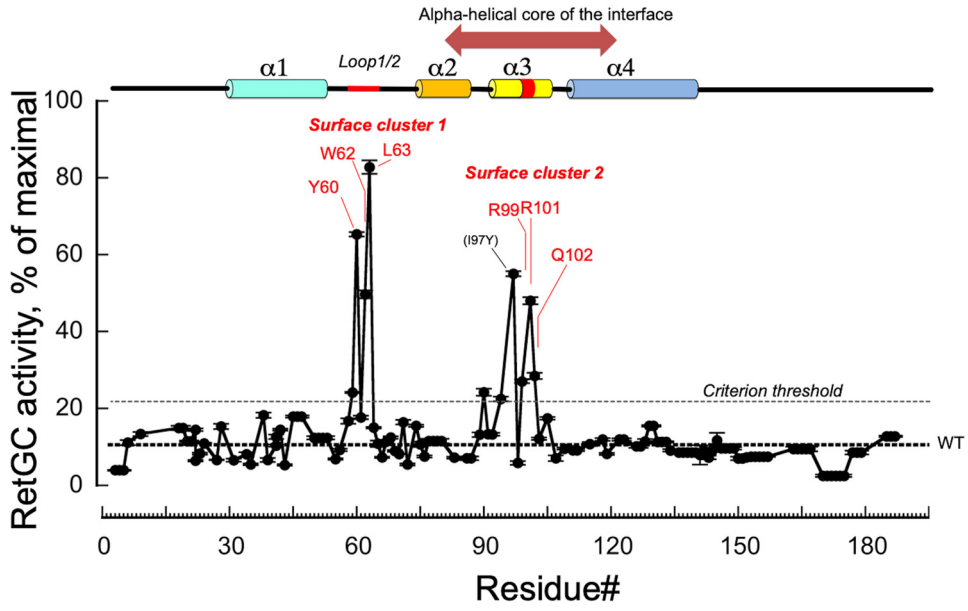

Figure 2. Point mutations in RD3 reveal two surface-exposed clusters affecting inhibition of RetGC1/GCAP1 complex. Purified 100 nM human RD3 containing mutations (see Table 1) in the corresponding positions of the residues numbered according to their sequence in the RD3 primary structure, beginning with Met[1], was added to the assays containing membranes isolated from HEK293 cell-expressing human recombinant RetGC1 reconstituted with 1.5 μM GCAP1 in the presence of 2 mM EGTA and 10 mM Mg^{2+}. The cyclase activity (mean ± S.D., three measurements) remaining in the presence of RD3 is plotted as percentage of the activity measured in the absence of RD3. The *thick dashed line* corresponds to the average cyclase activity remaining in the standard assay after inhibition by 100 nM WT RD3. The mutations at the surface-exposed side chains causing the strongest loss of inhibition (≥ 22% residual activity criterion threshold, *thin dashed line*) are shown in *red*, except for the Ile^{97} side chain only partially exposed on the surface and mostly located inside the core between helices 1 and 3. The *top diagram* presents the location of the respective clusters in the primary structure (*red*); the large *double-sided arrow* above the diagram indicates the span of the primary structure forming the interface-containing helical core of the bundle (24, 27).

by ~89% (Fig. 2 and Table 1). As a threshold for identifying mutants with a strong reduction in the inhibitory activity we selected a 2-fold reduction in the extent of the cyclase inhibition by WT RD3, *i.e.* the remaining cyclase activity ≥ 22%.

The results in Fig. 2 and Table 1 demonstrated that although substitutions of vast majority of the surface residues in RD3 had little effect on the ability of RD3 to suppress the cyclase activity, two narrow clusters, each containing only several surface-exposed side chains, presented a stark exception. The first cluster included previously untested part of the molecule occupying central portion of the loop that connects helices α1 and α2 in the central helical bundle structure. This part of the loop presented several hydrophobic side chains exposed on the surface: Tyr^{60}, Trp^{62}, and Leu^{63}. Even substitutions with other hydrophobic residues, such as Y60A or W62A, were most detrimental for the ability of RD3 to inhibit the cyclase. The second cluster critical for the cyclase inhibition was located on the surface of the helix α3 (Fig. 2) and included fully exposed highly hydrophilic side chains Arg^{99}, Arg^{101}, and Gln^{102}. This helix was shown previously to be an essential part of RD3 three-dimensional structure that folds the interface for binding to the cyclase (24, 27). Ile^{97}, closely adjacent to the surface-exposed residues in this cluster, also had a profound negative effect on the cyclase inhibition by RD3 when substituted with a large Tyr residue (Fig. 2). Nonetheless, the Ile^{97} is only partially exposed on the surface and remains mostly buried inside the helical bundle, hence the substitution of this side chain could also create a structural hindrance, altering the proper alignment between the α3 and α1 helices, similarly to previously tested residues buried in the core structure (24, 27), and thus affect the neighboring surface interface indirectly. Therefore, we cannot draw a conclusion that Ile^{97} is directly involved in contacting the cyclase. The same relates to Pro^{90}, a residue that could potentially affect not only interaction with the cyclase, but also the proper fold of the interface. In contrast, Arg^{99}, Arg^{101}, and Gln^{102} do not directly push on the backbone of other helices. Hence, the reduction of the RD3 inhibitory activity after mutating those residues indicated that they most likely constitute the surface part of the interface directly interacting with the cyclase.

The two clusters of surface-exposed residues define the high affinity of RD3 for the cyclase

The reduction in the inhibitory capacity of RD3 caused by mutations in the two surface-exposed clusters demonstrated in the standard assay (Fig. 2) could have two different explanations, either being a result of RD3 losing its binding affinity for the cyclase or a result of RD3 binding to RetGC without inhibiting the cyclase activity. Therefore, we tested the apparent affinities of various mutants for the cyclase by comparing the dose dependence of the cyclase inhibition by individual mutants to that of the WT RD3 (Fig. 3). We identified three fairly distinct groups of the mutants demonstrating different apparent affinities for the RetGC based on their dose dependence curves. Consistent with the results of the initial mutational scanning of the surface of the molecule in a standard assay at a fixed 100 nM RD3 (Fig. 2), the vast majority of the RD3 mutants (from the pool shown in *plain text* in Table 1) did not demonstrate reduction of the apparent affinities for the cyclase (Fig. 3, *A* and *B*). For a large group of such 62 tested mutants, the dose dependence of the cyclase inhibition was not shifted to the

Table 1

RetGC1 Activity in the presence of RD3 mutants. RetGC1 pre-activated by 1.5 μM Mg^{2+} GCAP1 was assayed as described in "Experimental procedures" in the presence of 100 nM RD3, and cyclase activity was normalized as percentage of its activity measured in the absence of RD3. The RD3 mutants for which the remaining cyclase activity was at least 2-fold higher than in the WT are *highlighted in bold*; all highlighted mutants were significantly different from the WT ($P < 0.0001$, Student's *t* test)

Mutation	% of Remaining GC Activity, *n*
WT	11 ± 1.2,19
^{3}L→S^{5} deletion	3.9 ± 0.1, 3
W6L	11.1 ± 0.6, 3
W6L/W9L	13.4 ± 0.6, 3
T18D/R19A	14.9 ± 0.6, 3
S20Y/P21R	11.5 ± 0.2, 3
A22Y	14.4 ± 0.3, 3
A22E	6.4 ± 0.2, 3
E23R	8.2 ± 0.3, 3
M24D	10.9 ± 0.1, 3
E27R	6.6 ± 0.1, 3
T28R	15.3 ± 0.7, 3
M31R	6.6 ± 0.4, 3
T34Q	8.1 ± 0.6, 3
G35Y	5.5 ± 0.2, 3
R38S	18.2 ± 0.7, 3
E39R	6.6 ± 0.5, 3
E41A	10.3 ± 0.3, 3
E41R	12.6 ± 0.6, 3
R42E	14.5 ± 0.3, 3
Q43R	5.3 ± 0.2, 3
^{45}RER^{47}→^{45}AAA^{47*}	17.9 ± 0.3, 3
^{50}AVRK^{53}→^{50}KAIE^{53*}	12.4 ± 0.4, 3
C55D	6.9 ± 0.2, 3
T56H	9.2 ± 0.3, 3
V58Q	16.7 ± 0.7, 3
D59R	**24.1 ± 0.2**, 3
Y60A	**65.3 ± 0.6**, 3
S61Y	17.7 ± 0.4, 3
W62A	**49.7 ± 1**, 3
L63R	**82.8 ± 1.8**, 3
A64R	15 ± 0.2, 3
S65Y	10.8 ± 0.8, 3
T66K	7.3 ± 0.2, 3
P67D	11 ± 0.6, 3
P67G	11.3 ± 0.5, 3
R68D	12.4 ± 0.3, 3
S69Y	9.0 ± 0.2, 3
T70R	8.2 ± 0.04, 3
Y71G	15.4 ± 0.3, 3
Y71E	16.4 ± 0.6, 3
D72R	5.5 ± 0.3, 3
S74R	15.5 ± 0.3, 3
P75R	10.7 ± 0.7, 3
I76R	7.5 ± 0.3, 3
^{77}ERLQ^{80}→^{77}QLRE^{80*}	11.5 ± 0.6, 3
D83R	7.2 ± 0.3, 3
V86R/K87A	7.1 ± 0.5, 3
H89G	13.2 ± 0.6, 3
P90A	**24.2 ± 0.9**, 3
S91Y	13.3 ± 0.1, 3
Y92A	13.3 ± 0.4, 3
G94Y	**22.5 ± 0.6, 3**
I97Y	**55 ± 0.6**, 3
L98R	5.9 ± 0.5, 3
L98Y	9.9 ± 0.2, 3
R99E	**27.1 ± 0.5**, 3
R101E	**37.9 ± 0.3**, 3
R101A	**48 ± 0.9**, 3
Q102L	**28.5 ± 0.8**, 3
L103R	12.1 ± 0.3, 3
A105R	8.5 ± 0.2, 3
A105Y	17.9 ± 0.2, 3
E106K	17.5 ± 0.3, 3
E108K	7.1 ± 0.8, 3
E110R	9.6 ± 0.2, 3
Q112E/E113Q	9.2 ± 0.2, 3
Q116Y	10.8 ± 0.5, 3
R119S	12.0 ± 0.3, 3
S120Y	8.2 ± 0.3, 3
Q123E/E124Q	11.9 ± 0.3, 3
E127R/R128E	10.1 ± 0.4, 3
^{132}EEE^{134}→^{132}QQQ^{134*}	11.8 ± 0.3, 3
A135R	9.1 ± 0.3, 3
^{137}KLTRQ^{141}→^{137}QRKTL^{141*}	8.6 ± 0.3, 3
W142A	7.9 ± 2.5, 3
S143Y	9.1 ± 0.2, 3
L144W	7.3 ± 0.5, 3
R145D	9.2 ± 0.05, 3
P146ter	11.7 ± 1.9, 3
^{147}RGSL^{150}→^{147}GRLS^{150*}	9.6 ± 0.3, 3
A151R/T152Q	7.1 ± 0.5, 3
F153R	7.3 ± 0.1, 3
^{154}KTRAR^{158}→^{154}ENSES^{158*}	7.5 ± 0.1, 3
^{164}SDIRT^{168}→^{164}RSDTI^{168*}	9.5 ± 0.6, 3
^{171}EDVERD^{176}→^{171}KKAKQR^{176*}	2.5 ± 0.3, 3
^{178}PPP^{180}→^{178}AAA^{180*}	8.5 ± 0.5, 3
^{186}SMP^{188}→^{186}PRS^{188*}	12.7 ± 0.2, 3

*Mutants from Ref. 24.

higher concentrations compared with the WT (note that because of the multitude of the mutants in that group only the combined family of their dose dependence curves are plotted in Fig. 3*B* in *gray*, without specifying the symbols for individual mutants). Even drastic changes in some of the well-conserved parts of the molecule did not produce a discernible reduction of the apparent binding affinity. Mutations in conserved N-terminal Trp residues or a large, 49-residue-long, deletion of the C-terminal fragment (Fig. 3*A*) (as well as deletion of an N-terminal Leu^{3}-Ser^{5} fragment, not shown), did not alter the apparent affinity of the RD3 inhibitory binding to the cyclase. The respective IC_{50} values for the WT, W6L/W9L, and 146ter RD3 were 3.6 ± 0.52 nM (mean ± S.D., $n = 19$), 4.5 ± 1.2 ($n = 3$), and 3.4 ± 0.8 nM ($n = 3$) (not statistically significant by Student's *t* test: $p = 0.28$ and 0.8, respectively). In contrast, mutations of the residues located in clusters 1 and 2 and their vicinity prominently shifted the dose dependence curves to higher concentrations (Fig. 3, *C* and *D*). The loss of the apparent affinity was strongest for substitutions of the residues occupying the central positions in each cluster (Fig. 3*C*). Mutations in Tyr^{60}, Trp^{62}, and Leu^{63} (cluster 1) or Arg^{101} and Gln^{102} (cluster 2) caused a drastic, up to 240-fold, reduction in the apparent affinity of RD3 for the cyclase compared with the WT (Fig. 3*C* and Table 2, also marked *red* in Fig. 4) (ANOVA $p < 0.0001$, F = 789; Bonferroni post hoc test at CL = 99% and $\alpha = 0.01$ yields *p* values between <0.0001 and 0.0235). Along with that, mutations neighboring the centers of the clusters, Asp^{59}, Ser^{61}, and Ser^{74} adjacent to Tyr^{60}-Leu^{63} in cluster 1 or His^{89}, Gly^{94}, Arg^{99}, Ala^{105} adjacent to Arg^{101}-Gln^{102} in cluster 2 (Fig. 3*D*, also marked *orange* in Fig. 4), reduced the apparent affinity ~3- to 10-fold (ANOVA $p < 0.0001$, F = 107; the Bonferroni post hoc test *p* values for differences from WT between <0.0001 and 0.016). For the majority of the surface mutations within the clusters 1 and 2, the increase in IC_{50} was also highly significant when compared with WT using Student's *t* test (Table 2). Notably, the critical residue in cluster 2, Arg^{101}, was highly sensitive to both the reversal of a charge (R101E) and the replacement with a small hydrophobic side chain (R101A) (Table 1 and 2), suggesting that this side chain is essential for the direct contact with the cyclase. In contrast, Ala^{105}, a less critical residue proximal to the Arg^{101}, was sensitive to replacement with a larger

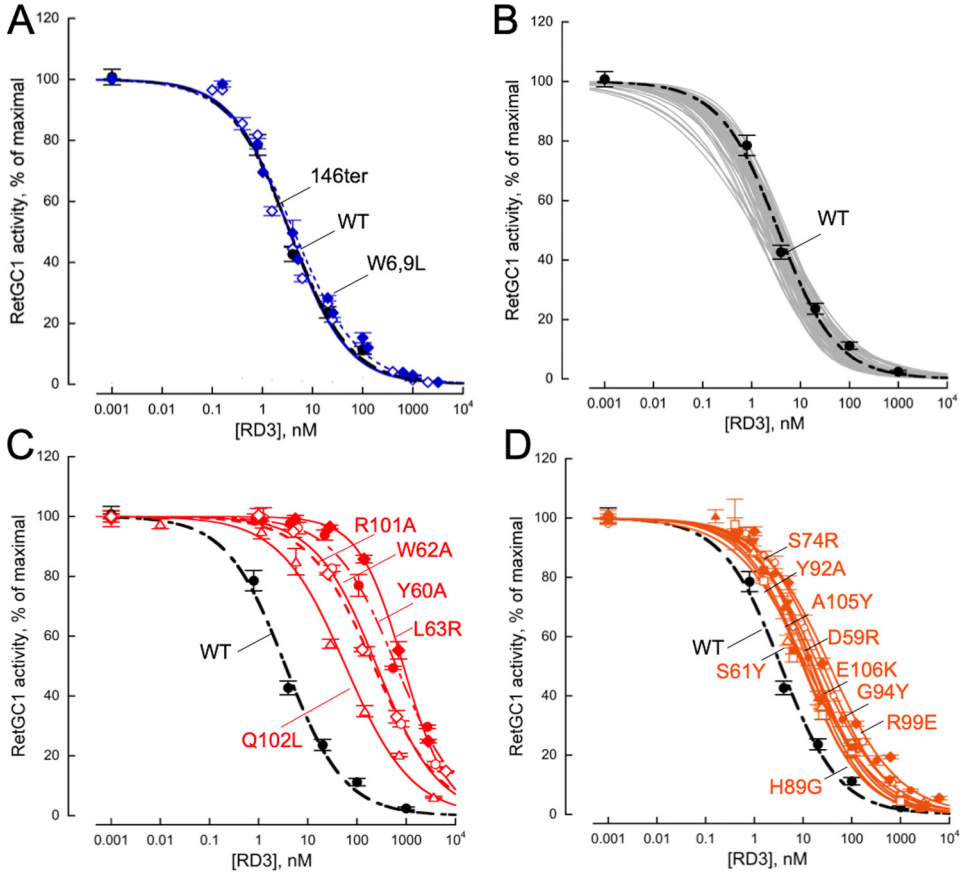

Figure 3. The effects of mutations on dose dependence of RetGC inhibition by RD3. The activity of RetGC in HEK293 cell membranes reconstituted with 1.5 μM GCAP1 (mean ± S.D., $n = 3$ independent experiments) was measured in the presence of increasing RD3 concentrations and plotted as percentage of the activity in the absence of RD3. The data were fitted assuming a sigmoidal function, $A_{\%} = 100\%/(1 + [RD3]/(IC_{50})^{-h})$, where A is the cyclase activity, [RD3] is the concentration of RD3 in the assay, and h is the Hill coefficient. *A*, the dose dependence of RetGC1 inhibition by WT (*black filled circle*), W6,9L (*blue filled wide diamond*), and 146ter RD3 (*blue open wide diamond*). Note the lack of right shift after replacing conserved N-terminal Trp residues or removal of the 49 residues from the C terminus. *B*, the dose dependence of WT RD3 (*black filled circle*), superimposed on those from a larger family of 62 mutations (ΔLys^3-Ser^5, W6L, T18D/R19A, A22E, A22Y, E23R, E27R, T28R, M31R, T34Q, R38S, E39R, E41R, R42E, Q43R, T56H, V58Q, S61Y, A64R, S65Y, T66K, P67G, P67D, R68D, S69Y, T70R, Y71G, Y71E, D72R, P75R, D83R, V86R/K87A, S91Y, L98R, L98Y, L103R, E108K, E110R, Q112E/E113Q, Q116Y, R119S, S120Y, Q123E/E124Q, E127R/R128E, K130Y/Q131W, A135R, W142A, S143Y, L144W, R145D, A151R/T151Q, F153R, I76R, *gray* lines) that fell below the threshold in the primary screening shown in Fig. 2 and Table 1. The symbols for the mutants were not plotted because of their multitude. *C*, surface mutations in RD3 (*red symbols*) causing a drastic shift in dose dependence of the inhibition: Y60A (*red filled circle*), W62A (*red open circle*), L63R (*red filled wide diamond*), R101A (*red open wide diamond*), Q102L (*red open triangle*); the corresponding IC_{50} values for these mutants are summarized in Table 2. *D*, surface mutations in RD3 (*orange symbols*) causing a moderate right shift in dose dependence from the WT (*black filled circle*): D59R (*orange open circle*), S61Y (*orange open triangle*), S74R (*orange open wide diamond*), H89G (*orange filled square*), Y92A (*orange open square*), G94Y (*orange filled circle orange*), R99E (*orange filled wide diamond*), A105Y (*orange filled triangle*), E106K (*orange filled inverted triangle*); the IC_{50} values for this group are summarized in Table 2.

side chain, Tyr, but not a more hydrophilic residue, Glu, which may indicate that this side chain is more important for proper presenting the neighboring Arg^{101} than for making a direct contact with the cyclase itself.

Taken together, the highly differential reduction of the apparent affinity of RD3 for the cyclase after mutating the large number of surface-exposed residues indicated that the functional interface for the RD3 inhibitory binding to the target enzyme requires two clusters located on the opposite sides of the central α-helical bundle surface (Fig. 4).

Mutations in both clusters had cumulative effect in reducing the RD3 inhibitory binding (Fig. 5). Compared with the single mutations (Fig. 3), second mutations in each cluster exacerbated the loss of the inhibitory activity. R101A/Q102L (cluster 2) shifted the IC_{50} ~1200-fold, to 4.5 μM from 3.6 nM in WT, stronger than either mutation alone (Figs. 3*C* and 5 and Table 2). In case of W62A/L63R (cluster 1) the effect was even more pronounced. Only rudimentary inhibition was observed by the double mutant at the RD3 concentrations exceeding 1 μM. Simultaneous inactivation of the two clusters of the interface (W62A/L63R + R101A/Q102L) completely eliminated the ability of the resultant Int(−) RD3 mutant to inhibit RetGC1 in the conditions of the assay (Fig. 5).

Inactivation of the binding interface on RD3 prevents co-localization of RD3 with RetGC

Based on the previous studies (24, 27), even RD3 mutants with reduced apparent affinity for the RetGC1/GCAP complex inhibition *in vitro* (IC_{50} increase up to ~1 μM) can co-localize with RetGC1 in HEK293 cells, evidently, because *in cyto* the absence of competing GCAPs (6, 23) helps RD3 bind the cyclase. However, more severe reduction in the apparent affinity of RD3 for RetGC1 in the *in vitro* inhibition assay also suppresses RD3 co-localization with the cyclase *in cyto* (24, 27).

Table 2

The change in IC_{50} of the RetGC1 inhibition by RD3 caused by mutations in clusters 1 and 2. The cyclase activity was assayed in the presence of 1.5 μM GCAP1, 2 mM EGTA, 10 mM Mg^{2+} and increasing concentrations of RD3 as described in Fig. 3, *C* and *D*, and "Experimental procedures." The IC_{50} values were obtained from the fits assuming sigmoidal function, $A_{\%} = 100\%/(1 + [RD3]/(IC_{50})^{-h})$, where *A* is the cyclase activity (100% in the absence of RD3), the [RD3] = concentration of RD3 in the assay, and *h* = the Hill coefficient. Statistically significant differences for IC_{50} (Student's *t* test) from WT are *highlighted in bold*

Mutation	IC_{50}, mean ± S.D. nM, *n*	P, Student's *t*
WT	3.6 ± 0.5, 12	–
Cluster 1		
Y60A	**630 ± 41**, 3	**0.0014**
W62A	**253 ± 18**, 3	**0.0018**
L63R	**882 ± 58**, 3	**0.0015**
W62A/L63R	Weak inhibition,* 3	N/A**
Cluster 2		
R101A	**261 ± 15**, 3	**0.0011**
R101E	**135 ± 18**, 3	**0.0064**
Q102L	**59 ± 7.4**, 3	**0.0059**
R101A/Q102L	**4457 ± 1556**, 3	**0.008**
Int(−) (Clusters 1 + 2)		
W62A/L63R + R101A/Q102L	No inhibition,* 3	N/A**
Cluster 1 vicinity		
D59R	**26.6 ± 3,** 3	**0.0055**
S61Y	**11.8 ± 0.82,** 3	**0.0015**
S74R	**15.6 ± 1.6**, 3	**0.0049**
Cluster 2 vicinity		
H89G	**10.6 ± 0.77**, 3	**0.0017**
Y92A	**9.8 ± 0.2**, 3	**0.0001**
G94Y	**20.7 ± 2.9**, 3	**0.0089**
R99E	**35.5 ± 4.2**, 4	**0.0006**
A105Y	**16.7 ± 3.2**, 3	**0.0183**
A105R	3.6 ± 0.4, 3	0.805
E106K	**13.5 ± 1.7**, 3	**0.0085**

*The IC_{50} value could not be obtained because of insufficient inhibition.
**Not applicable to this mutant because of lack of sufficient inhibition.

To further verify that the two clusters detected in the RetGC inhibition assay constitute the RD3 interface for binding to the cyclase, we co-expressed fluorescently tagged RD3-GFP variants with mOrange-tagged RetGC in HEK293 cells. Tagging RD3 by the fluorescent protein at the C terminus and RetGC1 with a tag replacing a portion of its N-terminal "extracellular" domain does not affect the function of either protein *in vitro* (24, 32–35). When expressed separately in HEK293 cells, RD3-GFP demonstrates a uniformly diffused distribution throughout the cytoplasm and the nuclei (except for nucleoli and vacuoles (24, 27, 35); mOrange-RetGC1, a transmembrane protein, displays clearly defined membrane localization primarily in the endoplasmic reticulum (32–35). Both proteins, however, co-localize in the membranes (Fig. 6*A*) when co-expressed using the conditions of the *in cyto* assay described in detail previously (24, 27, 35). Consistent with the functional assays presented in Figs. 2 and 3, the distribution of the GFP tag attached to WT RD3 or RD3 lacking 47 C-terminal residues ($\Delta_{148-195}$) across the cells coincided with the mOrange tag of the cyclase. The respective Pearson's correlation coefficients (PCC, mean ± S.D.), 0.90 ± 0.061 and 0.89 ± 0.051, confirmed strong co-localization with RetGC1 of the two RD3 variants, without a significant difference between them (Fig. 6, *A* and *B*) (note that PCC = 1.0 is the theoretical value for complete coincidence for both tags whereas PCC ≤ 0.5 indicates the lack of co-localization) (36). In stark contrast to the $\Delta_{148-195}$RD3, the Int(–) RD3 mutant (Fig. 6*C*), in which the interface for the cyclase on the surface of the molecule was inactivated by point mutations in the two clusters (W62A/L63R and R101A/Q102L), failed to co-localize with the cyclase (PCC = 0.32 ± 0.18; $p < 0.0001$ compared with the WT by *t* test).

Notably, it required more than a single mutation in the binding interface to disrupt RD3 association with the RetGC1 *in cyto* (Fig. 7). Neither W62A nor L63R alone, despite their marked increase of the IC_{50} in the inhibition assay *in vitro* (Fig. 3 and Table 2), were able to abolish co-localization RD3 with the cyclase in living cells, albeit in the case of W62A co-localization was less clearly defined than in WT and in the case of L63R it became heavily compromised, evidenced by diffusion of RD3 nonanchored to the cyclase through the cytoplasm and karyoplasm (the respective PCC = 0.83 ± 0.074 and 0.65 ± 0.13, $p < 0.001$) (Fig. 7, *A* and *B*). Inactivation of the cluster 1 with the double mutation, W62A/L63R (Fig. 7*C*), disrupted co-localization (PCC = 0.48 ± 0.13, $p < 0.0001$) nearly as efficiently as in Int(−) RD3 (Fig. 6*C*) and consistently with a severe loss of inhibition by the double mutant in the cyclase inhibition assay (Fig. 5).

Discussion

RD3, through binding to the cyclase, evidently promotes RetGC trafficking from the inner to the outer segment (2–5) to maintain the proper level of cGMP synthesis there, yet, the molecular mechanism of this process is poorly understood. The second role of RD3 in photoreceptor physiology, to inhibit RetGC and its activation by GCAPs in the inner segment, is essential for the survival of photoreceptors (6, 22, 24); therefore, RD3 deficiency associates with LCA12, a congenital form of human blindness (1, 25), and rapid degeneration of photoreceptors in *rd3* mouse strain (1). Notably, some mutations in RetGC1 and GCAPs associated with dominant retinopathies weaken inhibition by RD3 of the RetGC1/GCAP1 complexes containing the cyclase or GCAP1 coded by the disease-coding alleles (29, 37). So the high-affinity inhibitory binding of the RD3 to the cyclase documented in previous studies (6, 23, 24) is the necessary step in both preventing the photoreceptor death and enabling its normal function.

Although much has been learned about the biochemical properties and regulatory pathways related to RetGC function in photoreceptors (17–21), much less is known about the tertiary and quaternary molecular structures of the complexes between RetGC and its regulatory proteins. The structures of the two main protein regulators for the cyclase, GCAPs and RD3, have been largely established (27, 38–40). The functional interface for the cyclase at a single-residue resolution was previously identified for GCAPs using mutational testing (33, 41). In the present study, we have now identified the surface-exposed residues on RD3 that are essential for its inhibitory binding to RetGC.

Our findings indicate that the interface for the high-affinity inhibitory binding of RD3 to the cyclase evidently involves two narrow clusters, one in the loop connecting helices 1 and 2 and the other on the surface of helix 3 (Figs. 3 and 4). The location of the second cluster on helix 3 was not very surprising, the

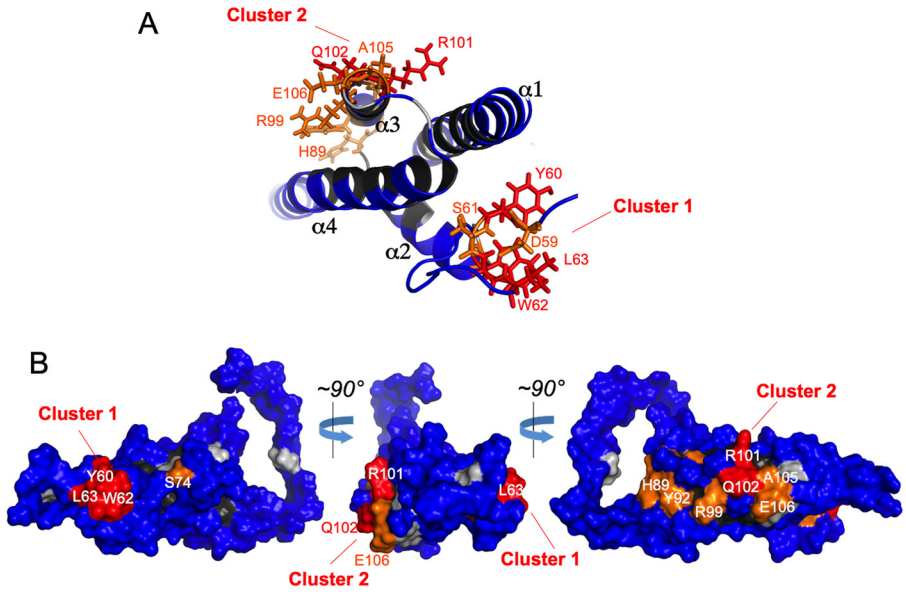

Figure 4. Location of the surface-exposed residues critical for the RD3 binding to the cyclase. *A*, the ribbon cartoon of the RD3 tertiary structure (27) depicting the two surface-exposed clusters that contain residues required for the high-affinity inhibitory binding of RD3 to the cyclase (with their side chains shown as *sticks*). The residues critically involved in the inhibitory binding are marked in *red* and those with a moderate involvement are marked in *orange*; the residues not critical for the high-affinity binding based on testing by point mutations in Fig. 2 are marked in *blue*. The internal residues not exposed on the surface are marked in *black*. *B*, space-filled RD3 three-dimensional structure depicts the location of the two respective clusters on the surface of the molecule.

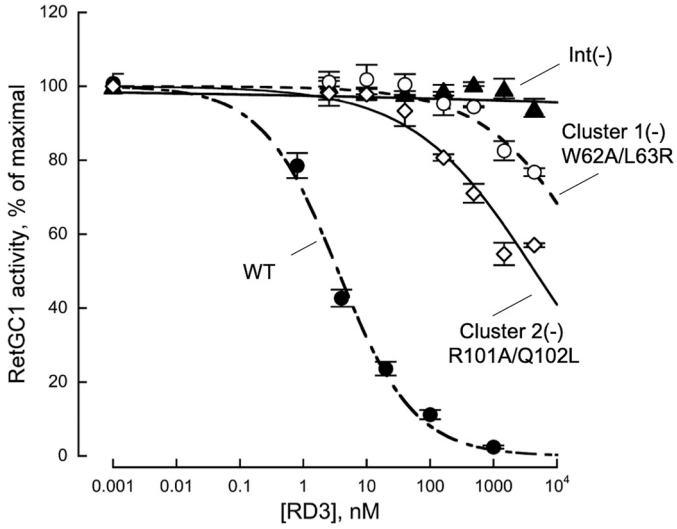

Figure 5. Inactivation of cluster 1 and cluster 2 in the cyclase-binding interface on RD3 completely abolishes the RetGC1 inhibition *in vitro*. The activity of RetGC in HEK293 cell membranes reconstituted with 1.5 μM GCAP1 (mean ± S.D., n = 3) was assayed in the presence of WT (*black filled circle*), W62A/L63R (*black open circle*), R101A/Q102L (*black open wide diamond*), and Int(–) RD3 (*black filled triangle*) as described in Fig. 3 legend. Note that only rudimentary inhibition was detectable in case of W62A/L63R (cluster 1). An empirical estimate for its IC_{50} from the observed dose dependence exceeded 10 μM, but could not be determined more precisely because the inhibition failed to approach 50% even at highest concentrations achievable in the assay. The Int(–) RD3 demonstrated a complete lack of inhibition in the conditions of the assay. The IC_{50} value for the R101A/Q102L (cluster 2) was 4.5 ± 1.6 μM compared with 3.6 ± 0.5 nM in WT (see also Table 2).

essential role of helices 2, 3, and 4 in forming the central part of the interface was demonstrated by previous low-resolution mutational testing (24, 27). Yet, the location of cluster 1, which was missed during the previous lower-resolution search for the interface, was somewhat surprising. The main reasons why this part of the molecule was not previously tested for being a potential surface interface based on the RD3 primary structure (1, 14, 24) is that the critical hydrophobic residues of the cluster 1, Tyr^{60}, Trp^{62}, and Leu^{63}, would more likely appear as a part of the molecule's hydrophobic core. However, after the three-dimensional structure of RD3 core was established recently (27), it became evident that these side chains in loop 1/2 are, despite their hydrophobic nature, largely exposed on the surface (Figs. 1 and 4), which prompted us to include these residues in the present mutational analysis. This cluster is reminiscent of the cyclase-binding interface on the surface of GCAP1, which includes, in addition to hydrophilic residues, several surface-exposed strongly hydrophobic side chains (33). However, dissimilarly to the cyclase interface on GCAP1, which forms a single patch on one side of the molecule, the two clusters on RD3 responsible for the high-affinity cyclase binding locate on two opposite sides of the molecule (Fig. 4).

Binding to the cyclase becomes completely abolished by inactivation of both clusters of the interface in Int(–) RD3 (Figs. 5 and 6). Very low–affinity inhibitory binding to the cyclase can still be detected after inactivation of either cluster (Fig. 5), but inactivation of cluster 1 has especially strong effect and also interferes with RD3 binding to the effector enzyme *in cyto* nearly as effectively as the Int(–) (Fig. 7), suggesting that RD3 affinity for the target imparted by the cluster 1 is the highest between the two clusters.

Notably, the LCA12-linked mutations in human RD3 (Fig. 1, *top panel*) have been shown to create termination codons upstream of or within cluster 1 or cluster 2 (R38ter, E46ter, Y60ter, F100ter), as well as produce a truncating frameshift, p. E46Afs*83, or deletion in the central part of the molecule (1, 25, 42). Hence, all LCA12-causing mutations reported to date eliminate the cyclase-binding interface of RD3 and truncate the protein. Even truncation eliminating second cluster of the

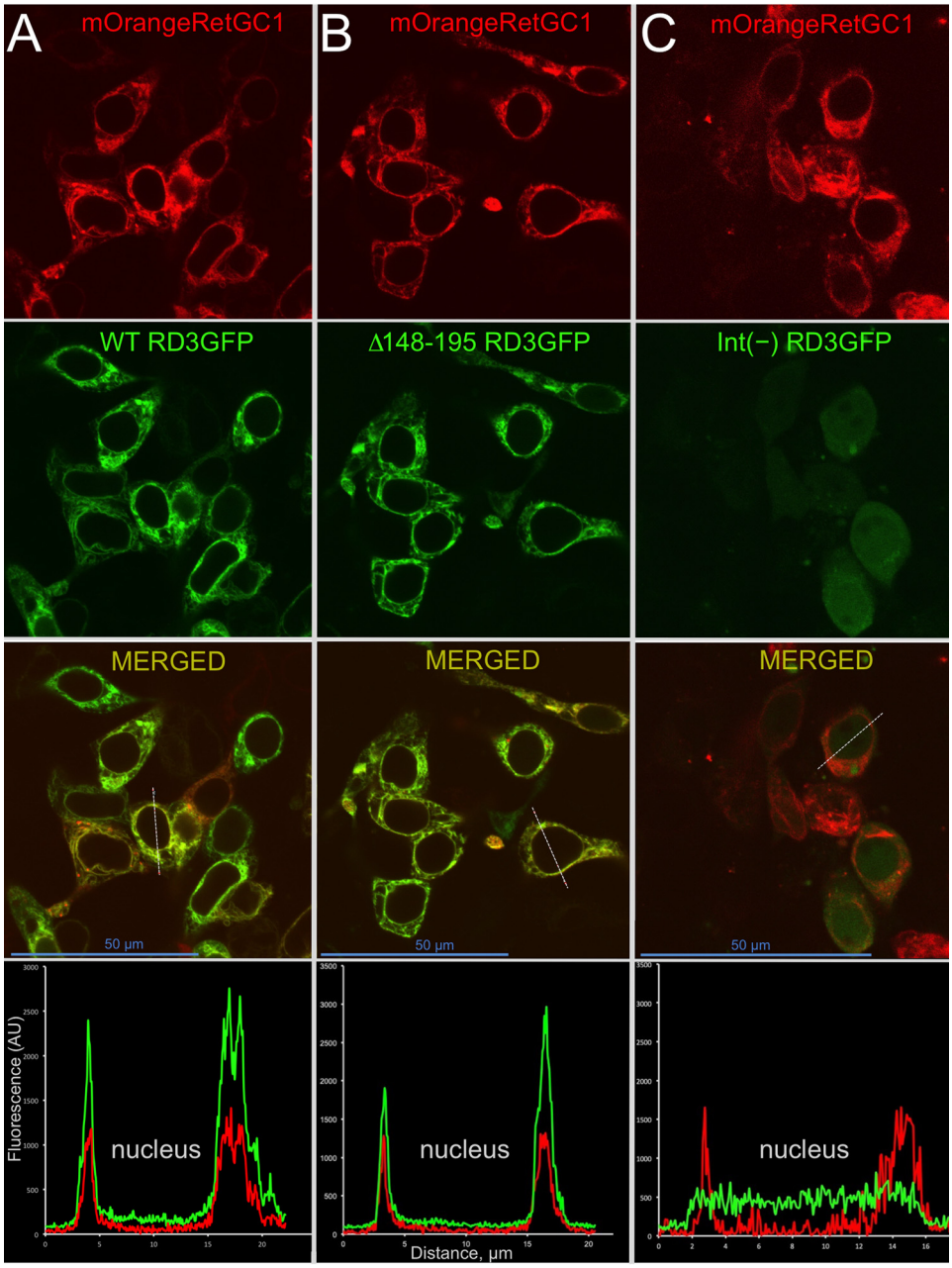

Figure 6. Inactivation of the cyclase-binding interface prevents RD3 association with RetGC1 in living cells. The representative images of mOrange-tagged RetGC1 (*red fluorescence*) transiently co-expressed in HEK293 cells with RD3 variants tagged at the C terminus with GFP (*green fluorescence*) *A–C*, WT (*A*), Δ148–195 (*B*), and Int(−) (*C*). The *bottom panel* in each column presents an example of distribution of the two respective fluorochromes across the cells when scanned in directions shown by *dashed lines* in the respective *merged* red/green fluorescence images. *Blue scale bars* = 50 μM. Note the characteristic "tennis racquet" (32, 35) co-localization pattern of RD3 with RetGC1 in (*A*) and (*B*) and the lack of such in (*C*), where Int(−) RD3 is uniformly spread throughout the cells. The respective PCC values (mean ± S.D.) for co-localization of the two fluorochromes in WT, Δ149–195, and Int(–) RD3 were 0.90 ± 0.061 (n = 33), 0.89 ± 0.051 (n = 42), and 0.32 ± 0.18 (n = 40). ANOVA $P < 0.0001$, $F = 329$; Bonferroni post hoc test (CL = 99%, $\alpha = 0.01$) showed high statistical significance of the differences between the Int(–) and the other two RD3 variants ($P < 0.0001$), but not between WT and Δ148–195 RD3 ($P = 1$).

interface, F100ter (1), completely disables inhibitory binding of RD3 to RetGC *in vitro* (23), despite the preservation of the cluster 1 in the remaining fragment of the polypeptide. Based on our present mutational analysis, it is also possible that LCA12 could result from yet to be found single-residue substitutions, but the occurrence of such missense mutations in RD3 would likely be even rarer than deletions found to date. The vast majority of surface-exposed side chains in RD3 tolerate replacement without affecting RD3 function (Figs. 2; 3, *A* and *B*; and 4). Therefore, to cause the disease, single-residue substitutions in RD3 would have to occur directly within the narrow clusters of the surface interface or deteriorate the fold of α-helical core of the interface (27).

Without knowing the detailed tertiary and quaternary structure of the cyclase we could at this point only speculate how the two clusters possibly make a connection with the enzyme. RetGC is a homodimer in which the catalytic domains of both subunits create the active site converting GTP to cGMP (43,

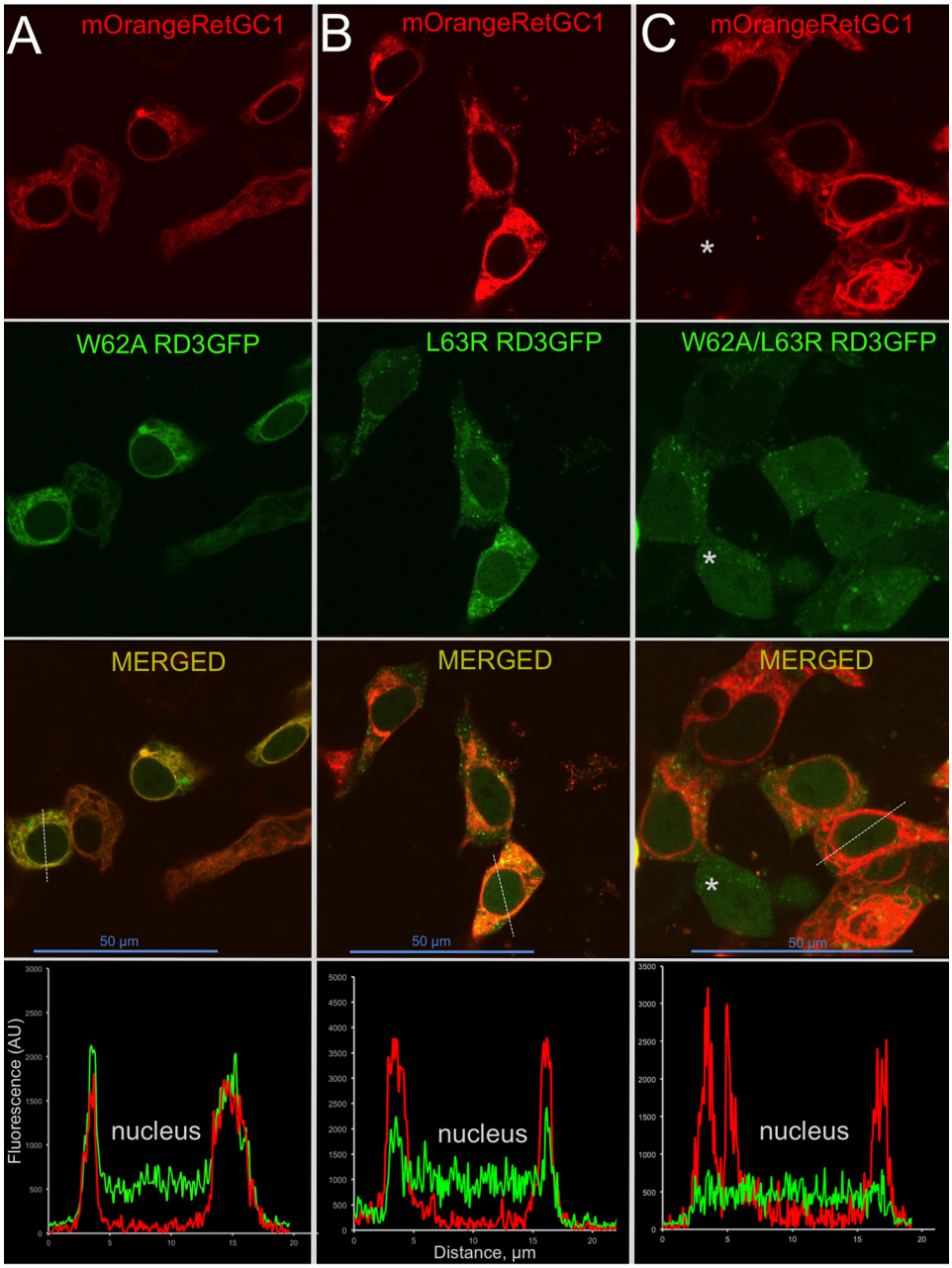

Figure 7. Cumulative effect of mutations in cluster 1 disrupts co-localization of RD3 and RetGC1 *in cyto*. The representative images of mOrange-tagged RetGC1 co-expressed with RD3 GFP variants, W62A (*A*), L63R (*B*), and W62A/L63R (*C*); distribution of the two fluorochromes along the *dashed lines* in the respective *merged* red/green fluorescence images is shown on the bottom. Note the residual co-localization in L63R and the absence of co-localization in W62A/L63R; the *asterisk* in *panel* C marks a cell lacking RetGC1 for comparison. *Blue scale bars* = 50 μM. The respective PCC values (mean ± S.D.) for the two fluorochromes were 0.83 ± 0.074 (n = 51), 0.65 ± 0.13 (n = 32), and 0.48 ± 0.13 (n = 40); ANOVA $P < 0.0001$, $F = 92$; Bonferroni post hoc test (CL = 99%, $\alpha = 0.01$) $P <$ 0.0001 indicated statistical significance of the differences between all three variants.

44). The inhibitory binding of RD3 to the cyclase displays a negative cooperativity, indicating possible involvement of at least two RD3 molecules in the complex (23, 24). Because RD3 is very prone to self-aggregation (23, 27), the negative cooperativity was previously regarded as a possible artifact produced by the aggregation of RD3 upon increase of its concentrations (24). However, a more recent study showed that a highly soluble form of RD3, not prone to aggregation, still demonstrated negative cooperativity in cyclase inhibition assay (27). Therefore, it is plausible that one molecule of RD3 can interact with two subunits of RetGC at the same time to create the inhibitory complex, in which it prevents the cyclase from being activated by GCAP. However, an alternative possibility—that each RD3 molecule interacts with two distant domains on a single RetGC1 subunit—cannot be excluded and at his point appears equally likely. The negatively cooperative inhibition in either case may indicate, for example, that binding of one RD3 per two cyclase subunits reduces the affinity for binding the second RD3 by the complex.

The mechanism of RetGC inhibition by RD3 and its competition with GCAP requires further functional and structural studies. GCAPs and RD3 compete against each other for the

cyclase (23, 24), but based on the mutational analysis of the RetGC1 (34, 35), this competition likely involves nonidentical sites on the cyclase. It is also important to emphasize that RD3 exerts its inhibitory binding on the cyclase directly, rather than, for example, through binding to and reducing the concentration of GCAPs, because (i) the RD3 inhibits the cyclase at concentrations that are ~500-fold lower than concentrations of GCAP in the assays (Table 1 and Figs. 2 and 3) (23, 24), and (ii) RD3 inhibits basal RetGC activity even in photoreceptor membranes completely devoid of GCAPs (23, 24). Whether or not the binding sites for GCAP and RD3 overlap in the tertiary and/or quaternary structure of the cyclase or affect each other allosterically by changing the overall shape of the cyclase in the complex remains to be further investigated.

Another aspect of the cyclase regulation by RD3 that requires further in-depth study is the apparent role of RD3 in delivering the cyclase to the outer segment (2–4). Although only a limited part of the RD3 structure is critical for making its high-affinity binding interface with RetGC (Fig. 4), other region(s) of the RD3 molecule could conceivably contribute to the intracellular trafficking of cyclase. For example, a small portion of the N-terminal or a large portion of the C-terminal unstructured regions can be removed from RD3 without any apparent loss of its high-affinity inhibitory binding to RetGC (Table 1 and Figs. 3 and 6), which appears to be somewhat at odds with the parts of these regions in RD3 primary structure being evolutionarily conserved (1, 2). Therefore, it is rather tempting to speculate that some of the conserved N- and/or C-proximal portions of the RD3 molecule are specifically required for the cyclase trafficking, such as by playing the role of a recognition signal or participating in the interactions with the trafficking machinery, after the high-affinity binding of RD3 to the cyclase has occurred via the interface identified in our present study. Experimental evaluation of such a possibility may also help shed light on additional biological processes potentially involving RD3, because some recent reports suggest that RD3 (or its homologs) can also interact with other trafficked or nontrafficked proteins (45, 46), and not only in the retina but also perhaps in different organs of vertebrate and invertebrate species.

Experimental procedures

Materials

Unless specified otherwise, nucleotides were purchased from Millipore/Sigma, chemicals (ultrapure or molecular biology grade) from Millipore/Sigma or Fisher Scientific, and restriction endonucleases from New England Biolabs.

RD3 mutagenesis, expression, and purification

Mutations were introduced in a human RD3 cDNA utilizing a conventional splicing by overlap extension technique (47), as described previously (6, 24, 27), using the cDNA's 5′-end coding and the 3′-end coding primers, 5′-AAGGACCATGGCTCTCATCTCATGGCTTCGGTGGAACGAGAAATT and 5′-GGATCCTCAGTCGGCTTTGGGCGCCCGGAAT, respectively, and primers that contained the designated nucleotide substitutions and at the same time generated overlapping regions for the subsequent splicing. The primary fragments were amplified in a PCR reaction using a human cDNA as a template and utilizing a Thermo Scientific Phusion Flash High-Fidelity DNA Polymerase. The fragments were then spliced in a second round of PCR using only the 5′-end and the 3′-end primers shown above. The spliced DNA constructs were purified using a Zymo Research DNA Clean-up Kit, digested with NcoI-HF and BamHI-HF endonucleases, inserted into the NcoI/BamHI sites of the pET11d vector (Novagen/Calbiochem), and amplified in a Zymo Research JM109 Mix & Go! *E. coli* strain, and minipreps isolated using a Promega Wizard Kit from 5-ml overnight cultures grown in the presence of ampicillin were verified by the automated DNA sequencing of the entire RD3 inserts in the resultant plasmids. To enable the use of the NcoI site for ligating the 5′-end of the constructs into the expression vector, the N-terminal Ser^2 was replaced by Ala in all bacterially expressed variants of RD3, a modification that does not interfere with the ability of RD3 to bind and inhibit RetGC (6, 23). For expression of a human RD3 tagged at the C terminus with SuperGlo eGFP (Clontech) in HEK293 cells, the cDNA was amplified using a forward primer, 5′-TTTTTTAAGCTT GGGCCAGGGGCTATGTCTCTCATCTCA and a reverse primer, 5′-AGCGGCAATTGTGAGTCGG CTTTGGGCGC-CCGGAAT, digested with HindIII-HF and MfeI-HF endonucleases, and subcloned into the HindIII/EcoRI sites of a pQBIFn3 vector (Clontech). The original N-terminal residue, Ser^2, remained preserved in these constructs. In some cases, instead of PCR amplification, the mutations were introduced into fragments of the RD3 cDNA using chemical synthesis (service of Integrated DNA Technologies, Iowa City, IA) and ligated into the vectors described above using the appropriate restriction sites. The recombinant human RD3 was expressed from pET11d (Novagen/Calbiochem) vector in BL21(DE3) CodonPlus *E. coli* strain (Agilent Technologies), extracted from inclusion bodies, and purified as described previously (23, 27), with minor modifications as follows. Inoculated with a frozen stock, 5-ml bacterial cultures in a standard Luria broth (Thermo Fisher Scientific) were grown overnight in incubator shaker at 37℃, 200 rpm, and then in 100-ml culture to reach A_{600} 0.6–0.7. The protein expression was induced by 1 mM isopropyl-β-D-thiogalactopyranoside for 2 h. The bacterial cell pellet was harvested by centrifugation at 7000 rpm for 10 min in a Sorvall Fiberlite F14-6 × 250y rotor at 4℃ and frozen in −70℃. The pellet was thawed, resuspended in 20 ml of 10 mM Tris-HCl, pH 7.5, 1 mM EDTA/14 mM 2-mercaptoethanol buffer solution (TEM) and sonicated on ice for 2 min using 2-s ultrasonic pulses. The inclusion bodies from the disrupted cells were collected by centrifugation at 22,000 × *g* for 10 min, 4℃, in a Sorvall Fiberlite F21-8 × 50y rotor. The pellet was resuspended in TEM, sonicated for 1 min on ice and centrifuged using the same regime. White pellet containing inclusion bodies was dissolved in 2.5 ml TEM buffer containing 2 mM EDTA and 8 M urea (BioXtra, Millipore/Sigma-Aldrich) by gentle stirring for 1 h at 4℃ and centrifuged at 22,000 × *g* for 10 min, 4℃. The supernatant was dialyzed in a Pierce/Thermo Scientific 3-ml 10,000 MWCO Slide-A-Lyzer Cassette G2 at 4℃ against 1 liter of TEM buffer containing 0.1 mM EDTA and 7 mM 2-mercaptoethanol for 3 h without stirring, then overnight against 1 liter of TEM containing 0.1 mM EDTA and 7 mM 2-

mercaptoethanol with gentle stirring and finally for 4 h against fresh 1 liter of the same buffer. RD3 was precipitated from the dialyzed protein fraction by adding NaCl to 250 mM. Precipitated protein was collected by centrifugation at 22,000 × *g*, 4°C, dissolved in TEM containing 8 M urea on ice and then dialyzed as described above, except that pH of TEM buffer was 8.3. The dialyzed protein solution was centrifuged at 5000 × *g* for 10 min at 4°C in a standard 2-ml Eppendorf tube, the supernatant was collected, and the protein concentration was measured by absorbance at 280 nm in 50 mM Tris-HCl, pH 7.5, containing 7 M guanidine chloride, assuming 0.1 g/liter absorbance 1.41 (calculated using a ProtParam software available online from the ExPASy server RRID:SCR_018087). The purity of the preparations was determined by SDS-PAGE in 15% gel, Coomassie Blue staining, and densitometry. For storage, the protein solutions were mixed with glycerol to final 35% v/v, aliquoted, frozen in liquid N_2, and stored in −70°C. Each aliquot was thawed only once, immediately before use in the RetGC assay. The final RD3 concentrations in the stock solutions typically varied between 5 and 50 μM.

GCAP1 expression and purification

Myristoylated bovine GCAP1 for *in vitro* assays was expressed from pET11d vector in a BLR(DE3) *E. coli* strain (both originated from Novagen/Calbiochem) harboring a pBB131 plasmid coding for a yeast *N*-myristoyl transferase and purified by calcium precipitation, butyl-Sepharose, and Sephacryl S-100 chromatography using previously published procedure (31–33). The purity of GCAP1 preparations estimated by SDS gel electrophoresis was ≥ 90%.

RetGC1 expression and activity assay

Human recombinant RetGC1 was expressed from a modified Invitrogen pRCCMV vector in HEK293 cells transfected using calcium-phosphate precipitation method, and the membrane fraction containing the expressed cyclase was purified as described previously (34). The guanylyl cyclase activity was assayed as described in detail previously (30, 48), with modification described (27). In brief, the assay mixture (25 μl) containing HEK293 membranes, 30 mM MOPS-KOH, pH 7.2, 60 mM KCl, 4 mM NaCl, 1 mM DTT, 2 mM EGTA, 10 mM Mg^{2+}, 0.3 mM ATP, 4 mM cGMP, 1 mM GTP, and 1 μCi of [α-^{32}P]GTP (Perkin Elmer), 100 μM zaprinast and dipyridamole was incubated at 30°C for 30 min and the reaction was stopped by heat inactivation at 95°C for 2 min. The resultant [^{32}P]cGMP product was separated by TLC using fluorescently backed polyethyleneimine cellulose plates (Merck) developed in 0.2 M LiCl, cut from the plate and eluted with 0.5 ml 2 M LiCl in 20-ml scintillation vials, and the radioactivity was counted by liquid scintillation in 10 ml UniverSol mixture (MP Biochemicals). Data fitting was performed using Synergy KaleidaGraph 4 software.

Co-transfection and confocal imaging

HEK293 cells were transfected in LabTeck 4-well cover glass chamber with 1 μg of mOrangeRetGC1 DNA per well using 3 μl/μg DNA of the Promega FuGENE reagent following the protocol recommended by the manufacturer at ~1/100 molar ratio of RD3-GFP coding plasmid *versus* mOrangeRetGC1 coding plasmid as described (27, 35). Confocal images were taken after 24–32 h of incubation in 5% CO_2, 37°C, utilizing an Olympus FV1000 Spectral instrument using the respective 543 nm and 488 nm excitation for the red and the green fluorochromes in sequential mode and processed using Olympus FluoView FV10-ASW software as described previously (27, 32–35). No changes to the original images were made except for minor γ correction applied to whole image for more clear presentation in print. Quantitative analysis was performed using only original images, without γ corrections. PCC for testing co-localization of RD3-GFP with mOrange-tagged RetGC1 in whole-cell images was calculated using Olympus FluoView FV10-ASW software as previously described (32, 35).

Three-dimensional molecular visualization

The protein images were created using the RD3 coordinates recently established by NMR spectroscopy (27) (PDB ID 6DRF) using PyMOL Molecular Graphics System, Version 2.0, Schrödinger, LLC.

Statistics

Statistical significance of the differences was tested by ANOVA and unpaired/unequal variance *t* test using Synergy KaleidaGraph 4 software.

Data availability

All data referred to in this manuscript are contained within the manuscript.

Acknowledgments—We thank Eric Westerman for technical assistance at the beginning of this study.

Author contributions—I. V. P. and A. M. D. data curation; I. V. P. and A. M. D. formal analysis; I. V. P. investigation; I. V. P. and A. M. D. methodology; I. V. P. and A. M. D. writing-original draft; A. M. D. conceptualization; A. M. D. supervision; I. V. P. and A. M. D. funding acquisition; A. M. D. project administration; A. M. D. writing-review and editing.

Funding and additional information—This work was supported by NEI, National Institutes of Health Grant EY011522 (to A. M. D.), by Pennsylvania Department of Health CURE formula grant (to A. M. D.), and Salus University Research Fund (to I. V. P.). The content is solely the responsibility of the authors and does not necessarily represent the official views of the National Institutes of Health.

Conflict of interest—The authors declare that they have no conflicts of interest with the contents of this article.

Abbreviations—The abbreviations used are: RD3, retinal degeneration-3; ANOVA, analysis of variance; GCAP, guanylyl cyclase–activating protein; LCA, Leber's congenital amaurosis; PCC, Pearson's correlation coefficient; RetGC, retinal membrane guanylyl cyclase; CL, confidence level.

References

1. Friedman, J. S., Chang, B., Kannabiran, C., Chakarova, C., Singh, H. P., Jalali, S., Hawes, N. L., Branham, K., Othman, M., Filippova, E., Thompson, D. A., Webster, A. R., Andreásson, S., Jacobson, S. G., Bhattacharya, S. S., *et al*. (2006) Premature truncation of a novel protein, RD3, exhibiting subnuclear localization is associated with retinal degeneration. *Am. J. Hum. Genet*. **79,** 1059–1070 CrossRef Medline
2. Molday, L. L., Jefferies, T., and Molday, R. S. (2014) Insights into the role of RD3 in guanylate cyclase trafficking, photoreceptor degeneration, and Leber congenital amaurosis. *Front. Mol. Neurosci*. **7,** 44 CrossRef Medline
3. Azadi, S., Molday, L. L., and Molday, R. S. (2010) RD3, the protein associated with Leber congenital amaurosis type 12, is required for guanylate cyclase trafficking in photoreceptor cells. *Proc. Natl. Acad. Sci. U. S. A*. **107,** 21158–21163 CrossRef Medline
4. Molday, L. L., Djajadi, H., Yan, P., Szczygiel, L., Boye, S. L., Chiodo, V. A., Gregory-Evans, K., Sarunic, M. V., Hauswirth, W. W., and Molday, R. S. (2013) RD3 gene delivery restores guanylate cyclase localization and rescues photoreceptors in the Rd3 mouse model of Leber congenital amaurosis 12. *Hum. Mol. Genet*. **22,** 3894–3905 CrossRef Medline
5. Zulliger, R., Naash, M. I., Rajala, R. V., Molday, R. S., and Azadi, S. (2015) Impaired association of retinal degeneration-3 with guanylate cyclase-1 and guanylate cyclase-activating protein-1 leads to Leber congenital amaurosis-1. *J. Biol. Chem*. **290,** 3488–3499 CrossRef Medline
6. Dizhoor, A. M., Olshevskaya, E. V., and Peshenko, I. V. (2019) Retinal guanylyl cyclase activation by calcium sensor proteins mediates photoreceptor degeneration in an rd3 mouse model of congenital human blindness. *J. Biol. Chem*. **294,** 13729–13739 CrossRef Medline
7. Dizhoor, A. M., Lowe, D. G., Olshevskaya, E. V., Laura, R. P., and Hurley, J. B. (1994) The human photoreceptor membrane guanylyl cyclase, RetGC, is present in outer segments and is regulated by calcium and a soluble activator. *Neuron* **12,** 1345–1352 CrossRef Medline
8. Lowe, D. G., Dizhoor, A. M., Liu, K., Gu, Q., Spencer, M., Laura, R., Lu, L., and Hurley, J. B. (1995) Cloning and expression of a second photoreceptor-specific membrane retina guanylyl cyclase (RetGC), RetGC-2. *Proc. Natl. Acad. Sci. U. S. A*. **92,** 5535–5539 CrossRef Medline
9. Yang, R. B., Foster, D. C., Garbers, D. L., and Fülle, H. J. (1995) Two membrane forms of guanylyl cyclase found in the eye. *Proc. Natl. Acad. Sci. U. S. A*. **92,** 602–606 CrossRef Medline
10. Peshenko, I. V., Olshevskaya, E. V., Savchenko, A. B., Karan, S., Palczewski, K., Baehr, W., and Dizhoor, A. M. (2011) Enzymatic properties and regulation of the native isozymes of retinal membrane guanylyl cyclase (RetGC) from mouse photoreceptors. *Biochemistry* **50,** 5590–5600 CrossRef Medline
11. Koch, K. W., and Stryer, L. (1988) Highly cooperative feedback control of retinal rod guanylate cyclase by calcium ions. *Nature* **334,** 64–66 CrossRef Medline
12. Palczewski, K., Subbaraya, I., Gorczyca, W. A., Helekar, B. S., Ruiz, C. C., Ohguro, H., Huang, J., Zhao, X., Crabb, J. W., Johnson, R. S., Walsh, K. A., Gray-Keller, M. P., Detwiler, P. B., and Baehr, W. (1994) Molecular cloning and characterization of retinal photoreceptor guanylyl cyclase-activating protein. *Neuron* **13,** 395–404 CrossRef Medline
13. Dizhoor, A. M., Olshevskaya, E. V., Henzel, W. J., Wong, S. C., Stults, J. T., Ankoudinova, I., and Hurley, J. B. (1995) Cloning, sequencing, and expression of a 24-kDa Ca^{2+}-binding protein activating photoreceptor guanylyl cyclase. *J. Biol. Chem*. **270,** 25200–25206 CrossRef Medline
14. Imanishi, Y., Yang, L., Sokal, I., Filipek, S., Palczewski, K., and Baehr, W. (2004) Diversity of guanylate cyclase-activating proteins (GCAPs) in teleost fish, characterization of three novel GCAPs (GCAP4, GCAP5, GCAP7) from zebrafish (*Danio rerio*) and prediction of eight GCAPs (GCAP1-8) in pufferfish (Fugu rubripes). *J. Mol. Evol*. **59,** 204–217 CrossRef Medline
15. Mendez, A., Burns, M. E., Sokal, I., Dizhoor, A. M., Baehr, W., Palczewski, K., Baylor, D. A., and Chen, J. (2001) Role of guanylate cyclase-activating proteins (GCAPs) in setting the flash sensitivity of rod photoreceptors. *Proc. Natl. Acad. Sci. U. S. A*. **98,** 9948–9953 CrossRef Medline
16. Sakurai, K., Chen, J., and Kefalov, V. J. (2011) Role of guanylyl cyclase modulation in mouse cone phototransduction. *J. Neurosci*. **31,** 7991–8000 CrossRef Medline
17. Makino, C. L., Wen, X. H., Olshevskaya, E. V., Peshenko, I. V., Savchenko, A. B., and Dizhoor, A. M. (2012) Enzymatic relay mechanism stimulates cyclic GMP synthesis in rod photoresponse, biochemical and physiological study in guanylyl cyclase activating protein 1 knockout mice. *PLoS One* **7,** e47637 CrossRef Medline
18. Koch, K.-W., and Dell'Orco, D. (2015) Protein and signaling networks in vertebrate photoreceptor cells. *Front. Mol. Neurosci*. **8,** 67 CrossRef Medline
19. Fu, Y., and Yau, K.-W. (2007) Phototransduction in mouse rods and cones. *Pflugers Arch*. **454,** 805–819 CrossRef Medline
20. Pugh, E. N., Jr., Nikonov, S., and Lamb, T. D. (1999) Molecular mechanisms of vertebrate photoreceptor light adaptation. *Curr. Opin. Neurobiol*. **9,** 410–418 CrossRef Medline
21. Dizhoor, A. M., Olshevskaya, E. V., and Peshenko, I. V. (2010) Mg^{2+}/Ca^{2+} cation binding cycle of guanylyl cyclase activating proteins (GCAPs): Role in regulation of photoreceptor guanylyl cyclase. *Mol. Cell. Biochem*. **334,** 117–124 CrossRef Medline
22. Plana-Bonamaisó, A., López-Begines, S., Andilla, J., Fidalgo, M. J., Loza-Alvarez, P., Estanyol, J. M., Villa, P. D L., and Méndez, A. (2020) GCAP neuronal calcium sensor proteins mediate photoreceptor cell death in the rd3 mouse model of LCA12 congenital blindness by involving endoplasmic reticulum stress. *Cell Death Dis*. **11,** 62 CrossRef Medline
23. Peshenko, I. V., Olshevskaya, E. V., Azadi, S., Molday, L. L., Molday, R. S., and Dizhoor, A. M. (2011) Retinal degeneration 3 (RD3) protein inhibits catalytic activity of retinal membrane guanylyl cyclase (RetGC) and its stimulation by activating proteins. *Biochemistry* **50,** 9511–9519 CrossRef Medline
24. Peshenko, I. V., Olshevskaya, E. V., and Dizhoor, A. M. (2016) Functional study and mapping sites for interaction with the target enzyme in retinal degeneration 3 (RD3) protein. *J. Biol. Chem*. **291,** 19713–19723 CrossRef Medline
25. Perrault, I., Estrada-Cuzcano, A., Lopez, I., Kohl, S., Li, S., Testa, F., Zekveld-Vroon, R., Wang, X., Pomares, E., Andorf, J., Aboussair, N., Banfi, S., Delphin, N., den Hollander, A. I., Edelson, C., *et al*. (2013) Union makes strength, a worldwide collaborative genetic and clinical study to provide a comprehensive survey of RD3 mutations and delineate the associated phenotype. *PLoS One* **8,** e51622 CrossRef Medline
26. Kukekova, A. V., Goldstein, O., Johnson, J. L., Richardson, M. A., Pearce-Kelling, S. E., Swaroop, A., Friedman, J. S., Aguirre, G. D., and Acland, G. M. (2009) Canine RD3 mutation establishes rod cone dysplasia type 2 (rcd2) as ortholog of human and murine rd3. *Mamm. Genome* **20,** 109–123 CrossRef Medline
27. Peshenko, I. V., Yu, Q., Lim, S., Cudia, D., Dizhoor, A. M., and Ames, J. B. (2019) Retinal degeneration 3 (RD3) protein, a retinal guanylyl cyclase regulator, forms a monomeric and elongated four-helix bundle. *J. Biol. Chem*. **294,** 2318–2328 CrossRef Medline
28. Koch, K.-W. (1991) Purification and identification of photoreceptor guanylate cyclase. *J. Biol. Chem*. **266,** 8634–8637 Medline
29. Peshenko, I. V., Cideciyan, A. V., Sumaroka, A., Olshevskaya, E. V., Scholten, A., Abbas, S., Koch, K.-W., Jacobson, S. G., and Dizhoor, A. M. (2019) A G86R mutation in the calcium-sensor protein GCAP1 alters regulation of retinal guanylyl cyclase and causes dominant cone-rod degeneration. *J. Biol. Chem*. **294,** 3476–3488 CrossRef Medline
30. Peshenko, I. V., Moiseyev, G. P., Olshevskaya, E. V., and Dizhoor, A. M. (2004) Factors that determine Ca^{2+} sensitivity of photoreceptor guanylyl cyclase. Kinetic analysis of the interaction between the Ca^{2+}-bound and the Ca^{2+}-free guanylyl cyclase activating proteins (GCAPs) and recombinant photoreceptor guanylyl cyclase 1 (RetGC-1). *Biochemistry* **43,** 13796–13804 CrossRef Medline
31. Peshenko, I. V., and Dizhoor, A. M. (2006) Ca2+ and Mg2+ binding properties of GCAP-1. Evidence that Mg2+-bound form is the physiological activator of photoreceptor guanylyl cyclase. *J. Biol. Chem*. **281,** 23830–23841 CrossRef Medline
32. Peshenko, I. V., Olshevskaya, E. V., and Dizhoor, A. M. (2008) Binding of guanylyl cyclase activating protein 1 (GCAP1) to retinal guanylyl cyclase (RetGC1): The role of individual EF-hands. *J. Biol. Chem*. **283,** 21747–21757 CrossRef Medline

33. Peshenko, I. V., Olshevskaya, E. V., Lim, S., Ames, J. B., and Dizhoor, A. M. (2014) Identification of target binding site in photoreceptor guanylyl cyclase activating protein 1 (GCAP1). *J. Biol. Chem.* **289,** 10140–10154 CrossRef Medline
34. Peshenko, I. V., Olshevskaya, E. V., and Dizhoor, A. M. (2015) Evaluating the role of retinal membrane guanylyl cyclase 1 (RetGC1) domains in binding guanylyl cyclase-activating proteins (GCAPs). *J. Biol. Chem.* **290,** 6913–6924 CrossRef Medline
35. Peshenko, I. V., Olshevskaya, E. V., and Dizhoor, A. M. (2015) Dimerization domain of retinal membrane guanylyl cyclase 1 (RetGC1) is an essential part of guanylyl cyclase-activating protein (GCAP) binding interface. *J. Biol. Chem.* **290,** 19584–19596 CrossRef Medline
36. Zinchuk, V., and Zinchuck, O. G. (2011) Quantitative colocalization analysis of confocal fluorescence microscopy images. *Curr. Prot. Cell Biol.* **52,** 4.16.1–4.16.16 CrossRef Medline
37. Dizhoor, A. M., Olshevskaya, E. V., and Peshenko, I. V. (2016) The R838S mutation in retinal guanylyl cyclase 1 (RetGC1) alters calcium sensitivity of cGMP synthesis in the retina and causes blindness in transgenic mice. *J. Biol. Chem.* **291,** 24504–24516 CrossRef Medline
38. Ames, J. B., Dizhoor, A. M., Ikura, M., Palczewski, K., and Stryer, L. (1999) Three-dimensional structure of guanylyl cyclase activating protein-2, a calcium-sensitive modulator of photoreceptor guanylyl cyclases. *J. Biol. Chem.* **274,** 19329–19337 CrossRef Medline
39. Stephen, R., Bereta, G., Golczak, M., Palczewski, K., and Sousa, M. C. (2007) Stabilizing function for myristoyl group revealed by the crystal structure of a neuronal calcium sensor, guanylate cyclase-activating protein 1. *Structure* **15,** 1392–1402 CrossRef Medline
40. Stephen, R., Palczewski, K., and Sousa, M. C. (2006) The crystal structure of GCAP3 suggests molecular mechanism of GCAP-linked cone dystrophies. *J. Mol. Biol.* **359,** 266–275 CrossRef Medline
41. Ermilov, A. N., Olshevskaya, E. V., and Dizhoor, A. M. (2001) Instead of binding calcium, one of the EF-hand structures in guanylyl cyclase activating protein-2 is required for targeting photoreceptor guanylyl cyclase. *J. Biol. Chem.* **276,** 48143–48148 CrossRef Medline
42. Preising, M. N., Hausotter-Will, N., Solbach, M. C., Friedburg, C., Rüschendorf, F., and Lorenz, B. (2012) Mutations in RD3 are associated with an extremely rare and severe form of early onset retinal dystrophy. *Invest. Ophthal. Vis. Sci.* **53,** 3463–3472 CrossRef Medline
43. Liu, Y., Ruoho, A. E., Rao, V. D., and Hurley, J. H. (1997) Catalytic mechanism of the adenylyl and guanylyl cyclases: modeling and mutational analysis. *Proc. Natl. Acad. Sci. U. S. A.* **94,** 13414–13419 CrossRef Medline
44. Tucker, C. L., Hurley, J. H., Miller, T. R., and Hurley, J. B. (1998) Two amino acid substitutions convert a guanylyl cyclase, RetGC-1, into an adenylyl cyclase. *Proc. Natl. Acad. Sci. U. S. A.* **95,** 5993–5997 CrossRef Medline
45. Martínez-Velázquez, L. A., and Ringstad, N. (2018) Antagonistic regulation of trafficking to *Caenorhabditis elegans* sensory cilia by a retinal degeneration 3 homolog and retromer. *Proc. Natl. Acad. Sci. U. S. A.* **115,** E438–E447 CrossRef Medline
46. Wimberg, H., Janssen-Bienhold, U., and Koch, K.-W. (2018) Control of the nucleotide cycle in photoreceptor cell extracts by retinal degeneration protein 3. *Front. Mol. Neurosci.* **11,** 52 CrossRef Medline
47. Horton, R. M., and Pease, L. R. (1991) Recombination and mutagenesis of DNA sequences using PCR. in *Directed Mutagenesis: A Practical Approach* (McPherson, M. J., ed) pp. 217–250, Oxford University Press, Oxford, England
48. Peshenko, I. V., and Dizhoor, A. M. (2004) Guanylyl cyclase-activating proteins (GCAPs) are Ca^{2+}/Mg^{2+} sensors: implications for photoreceptor guanylyl cyclase (RetGC) regulation in mammalian photoreceptors. *J. Biol. Chem.* **279,** 16903–16906 CrossRef Medline